*Desalination and Water Treatment*
www.deswater.com
doi: 10.1080/19443994.2015.1006816

57 (2016) 238–245
January

Taylor & Francis
Taylor & Francis Group

# Hydrothermally prepared graphene-titania nanocomposite for the solar photocatalytic degradation of methylene blue

Betty Yea Sze Chang[a,1], Muhammad Shahid Mehmood[a,1], Alagarsamy Pandikumar[a,*], Nay Ming Huang[a,*], Hong Ngee Lim[b], Ab Rahman Marlinda[a], Norazriena Yusoff[a], Wee Siong Chiu[a]

[a]*Faculty of Science, Physics Department, Low Dimensional Materials Research Centre, University of Malaya, 50603 Kuala Lumpur, Malaysia, emails: pandikumarinbox@gmail.com (A. Pandikumar), huangnayming@um.edu.my (N.M. Huang)*
[b]*Faculty of Science, Department of Chemistry, Universiti Putra Malaysia, 43400 UPM Serdang, Selangor, Malaysia*

Received 5 October 2014; Accepted 16 November 2014

ABSTRACT

Reduced graphene oxide–titania (rGO–$TiO_2$) nanocomposites were prepared by hydrothermal method at different reaction temperatures and characterized by powder X-ray diffraction, transmission electron microscopy, micro-Raman spectroscopy, X-ray photoelectron spectroscopy, and photoluminescence spectroscopy techniques, respectively. The photocatalytic properties of the nanocomposites were investigated toward the degradation of methylene blue under natural sunlight. The rGO–$TiO_2$ shows better photocatalytic activity due to the extended visible light absorption, excellent adsorptivity, and effective electron transfer process than the other controlled photocatalysts. In addition, rGO–$TiO_2$ shows good sustainability after subjecting it to five consecutive cycles of photodegradation. This enhanced photocatalytic performance and good sustainability toward dye removal makes this rGO–$TiO_2$ nanocomposite as a potential candidate for wastewater treatment in textile and dyeing industries.

*Keywords:* Photocatalysis; Nanocomposite; Titania; Graphene; Water purification; Methylene blue

## 1. Introduction

Semiconductor-based photodegradation of organic pollutants has attracted massive attention during the past decades due to their unique optical and electric properties of semiconductor in environmental applications, including air purification, water disinfection, hazardous waste remediation, and water purification [1,2]. Among the various semiconductor photocatalysts, titania ($TiO_2$) is known to be the most promising candidate for the degradation of environmental contaminants due to its high photocatalytic activity [3,4]. Besides that, its biological and chemical

*Corresponding authors.

[1]Author's contributed equally.

*Presented at the International Conference on Business, Economics, Energy and Environmental Sciences (ICBEEES) 19–21 September 2014, Kuala Lumpur, Malaysia*

inertness, strong oxidizing power, cost effectiveness, and long term stability against photocorrosion and chemical corrosion further support the widespread use of $TiO_2$ as environmental photocatalysts [1–4]. However, the problems associated with high charge recombination ($e^-\ldots h^+$) phenomenon inherent to the $TiO_2$, and the large band-gap energy (3.2 eV) offers only the absorption of ultraviolet radiation for the activation of $TiO_2$ toward photocatalytic applications [5]. Researchers have made efforts to modify the $TiO_2$ by doping with metal [5] and nonmetals [6], coupling with another semiconductor [7] and secondary photoactive molecules [8], deposition of mono- and bimetallic nanoparticles [9,10], and making hybrid with carbonaceous materials including CNT, MWCNT, graphene, etc. [11,12].

Among the various carbonaceous materials, graphene has gained lot of attention in recent years due to its unique optical, electrical, thermal, mechanical, electrochemical, and photochemical properties. Since, it has a large theoretical specific surface area (2,630 $m^2\,g^{-1}$), high carrier mobility at room temperature (10,000 $cm^2\,V^{-1}S^{-1}$), good thermal conductivity (5,000 $Wm^{-1}\,K^{-1}$), and good optical transmittance (~97.7%) [12–14]. Owing to these advantages, graphene has been used as suitable support materials to immobilize the metal oxide semiconductor photocatalysts [12,15,16] which shows superior adsorptivity of the target substrate on immobilized catalyst, retardation in the charge recombination, and thereby increase the electron transfer process which led to the enhanced photocatalytic performance [12,15,16].

In this study, the reduced graphene oxide–titania (rGO–$TiO_2$) nanocomposites were synthesized by hydrothermal method at different temperature and characterized with suitable analytical techniques. The photocatalytic activity of the as prepared rGO–$TiO_2$ nanocomposites was studied toward the degradation of methylene blue (MB), as a model pollutant under natural sunlight. The rGO–$TiO_2$ exhibited excellent photocatalytic activity than the other controlled samples due to the increased adsorptivity, extended visible light absorption and reduced electron-hole recombination.

## 2. Experimental methods

### 2.1. Materials

Graphite flakes were purchased from Asbury Graphite Mill Inc. P25 and TTIP (99%) were received from Acros Organics. Triethanolamine (TEA) and potassium permanganate ($KMnO_4$) were obtained from R&M Chemicals (Malaysia). Chemical reagents, such as sulfuric acid ($H_2SO_4$), phosphoric acid ($H_3PO_4$), hydrogen peroxide ($H_2O_2$), and ethanol were purchased from Merck, Germany. MB was obtained from Systerm.

### 2.2. Synthesis of rGO–$TiO_2$ nanocomposites

The rGO–$TiO_2$ nanocomposite was synthesized according to the following procedure. Initially, GO was prepared by via a simplified Hummers method [17]. A 0.5 M of Ti(IV) solution was prepared separately by mixing a 3.72 mL of TTIP into a 3.32 mL of TEA in a volumetric flask and made up to 25 mL. In order to obtain rGO–$TiO_2$ nanocomposite, 10 mL of GO solution (1 mg/mL) was added into $H_2O$:EtOH mixture (1:14 *v*/*v*) under stirring and then 3 mL of Ti (IV) solution was added and allowed to stirred for 24 h at room temperature to obtain a homogeneous suspension and then, the mixture transferred into a teflon-lined autoclave and heated to 120˚C for 24 h. Finally, a black precipitate was obtained and washed three times with ethanol, centrifuged, and dried at 60˚C. Two more samples were also prepared by an identical procedure at the reaction temperature of 150 and 180˚C. The samples were denoted as 120-rGO–$TiO_2$, 150-rGO–$TiO_2$, and 180-rGO–$TiO_2$.

### 2.3. Characterization techniques

Micro-Raman spectroscopy (Raman) and photoluminescence (PL) spectral measurements were performed in a Renishaw in via Raman microscope with 514 nm and 325 laser excitation, respectively. The X-ray diffraction (XRD) analysis was carried out by -Siemen D5000 X-ray diffractometer with Cu K$\alpha$ radiation ($\lambda$ = 1.5418 Å). Morphological of rGO–$TiO_2$ nanocomposite was studied using JEOL JEM-2100F high resolution transmission electron microscopy (TEM). X-ray photoelectron spectroscopic (XPS) measurement was performed by using synchrotron light at beam line No. 3.2 of Siam Photon Laboratory, Synchrotron Light Research Institute, Thailand at maximum photon energy 600 eV, and kinetic energy step 0.1 eV.

### 2.4. Photocatalytic studies

The photocatalytic activity of prepared nanocomposite materials was evaluated by using MB as a standard reference dye. In a typical process, 10 mg of photocatalyst was dispersed into the 80 mL of MB dye solution (0.01 g/L, i.e. 10 ppm) under constant stirring. Before photocatalytic studies, the solution was stirred in the dark for 30 min to establish

adsorption-desorption equilibrium. After 30 min, photolysis cell was exposed into natural solar light irradiation. All the experiments were performed on bright sunny days between 9 am and 2 pm. At regular time intervals, the sample aliquots was periodically withdrawn from the photolysis cell and tested for dye degradation using UV–visible spectrophotometer (Thermo Scientific Evolution 300) by measuring the absorption intensity at 663 nm.

### 2.5. Dark adsorption and sustainability test

Dark adsorption of MB on the surface of photocatalysts was tested by dispersing 10 mg of catalyst into a 10 ppm of MB solution under stirring and kept in the dark for 10 min. And then, the dispersion was centrifuged and absorption spectra were recorded for the MB solution. Difference between the absorbance intensity, before and after adsorption, the amount of dyes adsorbed by the catalyst was estimated.The sustainability of the photocatalysts was studied by keeping the all experimental parameters were constant and the photocatalytic experiments were repeated for five sets using the same photocatalysts with fresh MB solution. After each photodegradation studies, the photocatalysts were removed by using centrifuge and then washed with high pure DI water in order to remove any organic contamination due to MB.

## 3. Results and discussion

### 3.1. Characterization studies

Raman spectroscopy is a powerful tool to study the disorder and defect structures of graphene. The typical Raman peaks observed at 1,346 and 1,598 $cm^{-1}$, corresponding to the D and G bands, respectively, for graphene (Fig. 1(a), (b), (d)). The D band is associated with the vibrations of carbon atoms with $sp^3$ electronic configuration of disordered graphene, while G band is related to the in-plane vibration of $sp^2$-bonded carbon atoms. The rGO exhibited a slight increase in the D/G band intensity ratio as compared to that in the GO spectrum. This change suggests that the decline in the average size of the in-plane $sp^2$ domain upon chemical reduction of the exfoliated GO sheets. It is reasonable to consider that the reduction of GO sheets causes fragmentation along the reactive sites and yields new graphitic domains, which led to the smaller size rGO sheets when compared to GO. The small size of rGO sheets will result in large number of edges and these edges will act as defects, consistent with the increase in the D band intensity [18]. The $TiO_2$ showed the four peaks at the

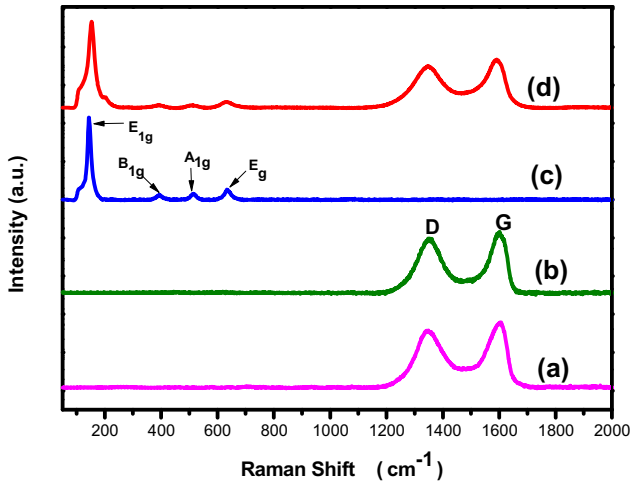


Fig. 1. Raman spectra obtained for as prepared (a) GO, (b) 180-rGO, (c) 180-$TiO_2$, and (d) 180-rGO–$TiO_2$.

low frequency region and are assigned to the $E_{1g}$ (149 $cm^{-1}$), $B_{1g}$ (398 $cm^{-1}$), $A_{1g}$ (516 $cm^{-1}$), and $E_g$ (637 $cm^{-1}$) modes of anatase phase, respectively [19,20]. The G and D bands in the Raman spectrum of rGO–$TiO_2$ are similar to those of rGO suggests that the introduction of $TiO_2$ nanoparticles did not affect the structure of the rGO sheets. Compared with GO, the rGO–$TiO_2$ nanocomposite showed an increased D/G intensity ratio and it suggests that a decrease in the average size of the $sp^2$ domains upon reduction of the exfoliated GO [21,22].

XPS is powerful tool used to confirm the formation of rGO from the reduction of GO through a hydrothermal method. Fig. 2 shows the high-resolution XPS spectra of the C1s region of 180-rGO–$TiO_2$ nanocomposite. The deconvoluted peak centered at 285.0 eV is assigned to the C–C and C=C bonds. In addition, the

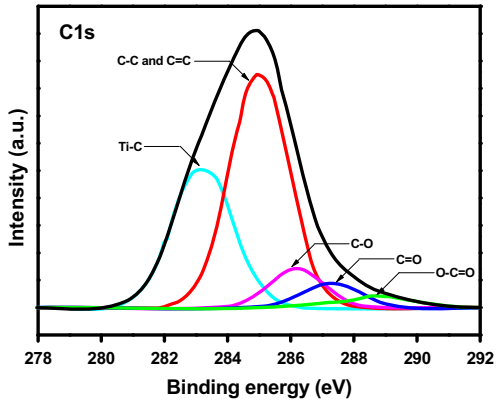


Fig. 2. XPS spectra of 180-rGO–$TiO_2$ nanocomposite.

peaks centered at 286.2, 287.3, and 288.5 eV are attributed, respectively, to the C–O, C=O, and O–C=O bonds [23,24]. On the other hand, the deconvoluted peak centered at 283.2 eV is due to the formation of Ti–C bond [25,26]. This result indicates that hydrothermal process led to the formation of Ti–C chemical bond between the carbon of the rGO and the Ti(IV) of the $TiO_2$ nanoparticles. The XPS analysis clearly indicates the strong interaction at interfaces between rGO and $TiO_2$ in the rGO–$TiO_2$ nanocomposite. The intense interaction lead in the creation of an electron transfer channel and it is more favorable to improve the photo-induced charge separation process during the photocatalytic reaction [27].

Fig. 3 shows the XRD patterns of the graphite, GO, rGO, pure $TiO_2$, and rGO–$TiO_2$ nanocomposites prepared at various hydrothermal temperatures. The dominant diffraction peak observed at the $2\theta$ value of 11° is corresponds to the (0 0 2) plane of GO [28] (Fig. 3(a)), whereas, the raw graphite flakes showed a high intense diffraction peak at the $2\theta$ value of 26°. The RGO shows the broad diffraction around the $2\theta$ value of 25° due to the (0 0 2) plane and the broad diffraction peak indicates poor ordering of the sheets along the stacking direction, which implies the sample was comprised mainly from single or only a few layers of rGO [29]. Another peak observed at 43° due to the turbo static band of disordered carbon materials [30]. No other diffraction peak was observed for graphite crystal, which suggests that the stacking of the rGO sheets remained disordered and were not stacked together to form a detectable graphite structure. In addition to the diffraction peaks of carbon-based compounds, the XRD peaks have been assigned to the anatase phase of tetragonal $TiO_2$ with lattice constants of $a = 3.7892$ Å, $b = 3.7892$ Å, $c = 9.5370$ Å, and $\beta = 90.0000$ (JCPDS 71-1167). The diffraction peaks can be indexed as (1 0 1), (0 0 4), (2 0 0), (1 0 5), (2 1 1), and (2 0 4) planes, respectively. There was no evidence for the other phases of $TiO_2$ being present. Comparing the 180-rGO–$TiO_2$ and the 120-rGO–$TiO_2$ samples, an increased in diffraction peak intensities for $TiO_2$ was observed for 180-rGO–$TiO_2$, which suggests the formation of larger $TiO_2$ crystallites and enhancement of the $TiO_2$ crystallization process [31]. Full width at half maximum (FWHM) of the $TiO_2$ (1 0 1) reflection for the 120-rGO–$TiO_2$, 150-rGO–$TiO_2$, and 180-rGO–$TiO_2$ samples was 1.1595°, 0.9832°, and 0.6378°, respectively. Since the FWHM is inversely proportional to the nanocrystal size (Scherrer equation), this result further confirms the hypothesis that higher hydrothermal temperatures can produce $TiO_2$ with better crystallization. The presence of graphene cannot be confirmed in the XRD for the rGO–$TiO_2$ samples due to weak and broad characteristic peak of graphene at 24.5° was masked by the strong (1 0 1) plane of $TiO_2$ at 25.4° [32].

TEM images of the prepared nanocomposites were recorded and are shown in Fig. 4 along with the histograms of the $TiO_2$ nanoparticles. It is clearly noted that the $TiO_2$ nanoparticles are distributed uniformly on the basal plane of rGO nanosheets. The $TiO_2$ nanoparticles appear to have a spherical shape in the 180-rGO–$TiO_2$ samples when compared to the 120-rGO–$TiO_2$ nanocomposite. The TEM for the different nanocomposites showed the average size of the $TiO_2$ nanoparticles for the 120-rGO–$TiO_2$, 150-rGO–$TiO_2$, and 180-rGO–$TiO_2$ are 20.4 ± 3.9, 20.5 ± 4.7, and 21.3 ± 3.5 nm, respectively. While increase in the temperature during the hydrothermal process, the size distribution of $TiO_2$ nanoparticles becomes narrow. The lattice resolved TEM image of $TiO_2$ indicates a well-defined crystallinity with lattice spacing of 0.349 nm, which corresponds to the (1 0 1) planes of anatase phase.

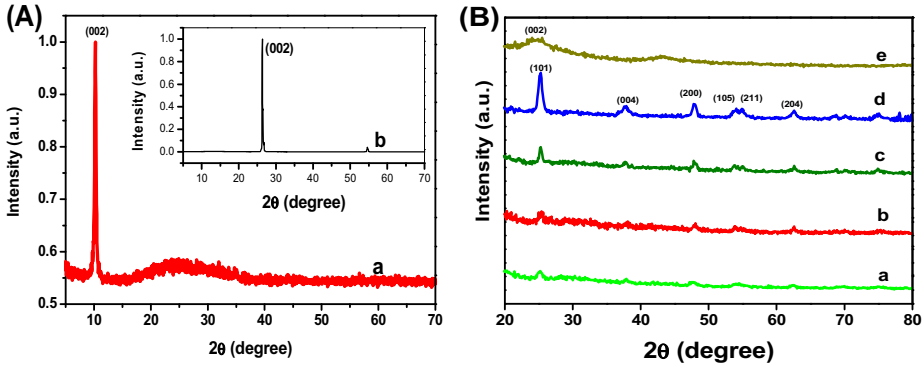


Fig. 3. (A) XRD patterns of (a) graphite and (b) GO. (B) XRD patterns of (a) 120-rGO–$TiO_2$, (b) 150-rGO–$TiO_2$, (c) 180-rGO–$TiO_2$, (d) 180-$TiO_2$, and (e) 180-rGO.

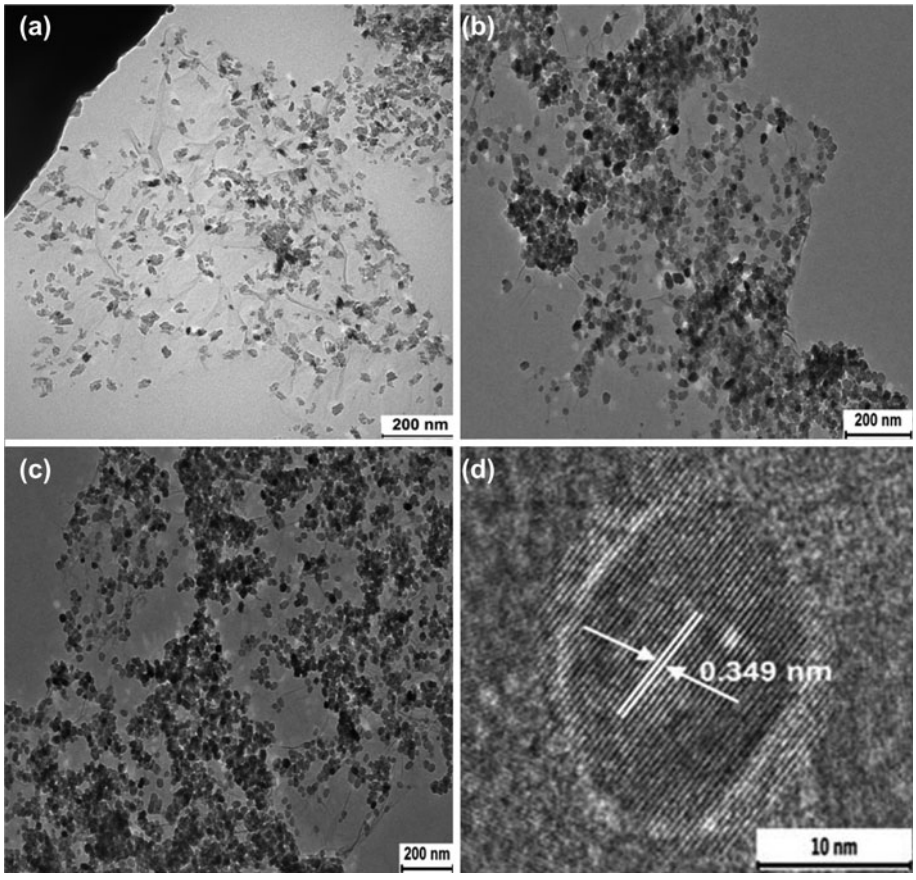


Fig. 4. TEM images obtained for the rGO–$TiO_2$ nanocomposites synthesized at (a) 120, (b) 150, and (c) 180˚C, respectively, and (d) lattice resolved TEM image of rGO–$TiO_2$ nanocomposites synthesized at 180˚C.

The PL spectra has been extensively utilized to study the surface structure and excited state of semiconductor [33,34]. Upon irradiation, the semiconductor undergoes electron-hole separation followed by the recombination leads PL. This phenomenon is due to the reverse radiative deactivation from the excited state of $TiO_2$. Fig. 5 shows PL spectra of P25, pure $TiO_2$, and rGO–$TiO_2$ nanocomposites prepared at three different temperatures. The P25 shows the broad and intense PL band than the 180-$TiO_2$. The rGO–$TiO_2$ nanocomposites exhibited an abrupt PL quenching of $TiO_2$, representing that rapid electrons transfer from excited $TiO_2$ to graphene. The inset is the expanded view in the range of 400–710 nm, implicating that the quenching extent is in relation to the hydrothermal temperature used. Increasing the hydrothermal temperature from 120 to 180˚C, the PL intensity decreased gradually. This result indicates that the recombination of photoinduced electrons and holes were suppressed by the rGO in the rGO–$TiO_2$ nanocomposites. Further, it shows that a typical charge separation at the surface junction and the electrons are tend to flow from the

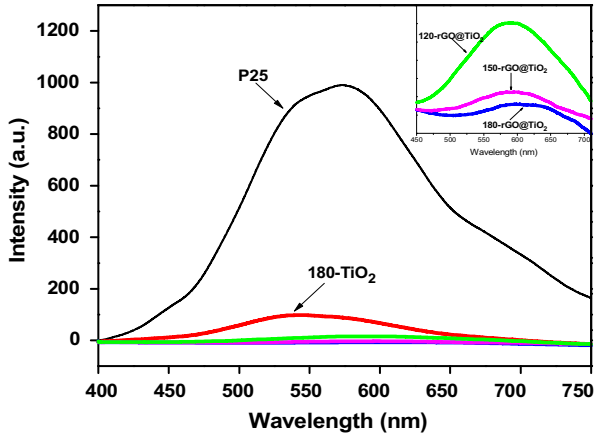


Fig. 5. PL spectra obtained for P25, pure $TiO_2$, 120-rGO–$TiO_2$, 150-rGO–$TiO_2$, and 180-rGO–$TiO_2$.

higher to lower Fermi level to adjust the Fermi energy levels [35]. As the calculated work function of graphene is 4.42 eV and the conduction band position of anatase is about −4.21 eV [36] with a band gap of

~3.2 eV (using vacuum level as a reference) [37] and it suggest that graphene can accept the photoexcited electrons from $TiO_2$, thus hinders the electron-hole recombination. It has been reported that heating treatment leads to the formation of titanium–carbon (Ti–C) bonds between graphene and $TiO_2$ [25,26]. Hence, increasing the reaction temperature promotes the bonding of $TiO_2$ on graphene with Ti–C bond, leading to better adhesion. Better linkage between the two materials must facilitate the electrons transfer, causing an abatement of emission.

### 3.2. Photocatalytic activity of rGO–$TiO_2$ nanocomposites

The photocataytic activities of the prepared rGO–$TiO_2$ nanocomposites were studied by choosing MB as a model pollutant under natural sunlight illumination. The photodegradation of MB was monitored by the change in the concentration ($C/C_0$) from the difference between the absorbance ($A/A_0$), where $C_0$ and $A_0$ are the initial concentration and absorbance of MB, respectively. After 10 min stirring the reaction solution in dark, ~50% of MB molecules were adsorbed on the rGO–$TiO_2$ photocatalysts surface (Fig. 6(A)). This is due to the great adsorptivity behavior of rGO–$TiO_2$ nanocomposite toward the MB molecules and which ~8-fold higher than the bare P25 and $TiO_2$ nanoparticles (data not shown due to brevity). The enhanced adsorption due to the non-covalent interaction, which is driven by the $\pi$–$\pi$ stacking between MB and aromatic regions of graphene, which was similar to the

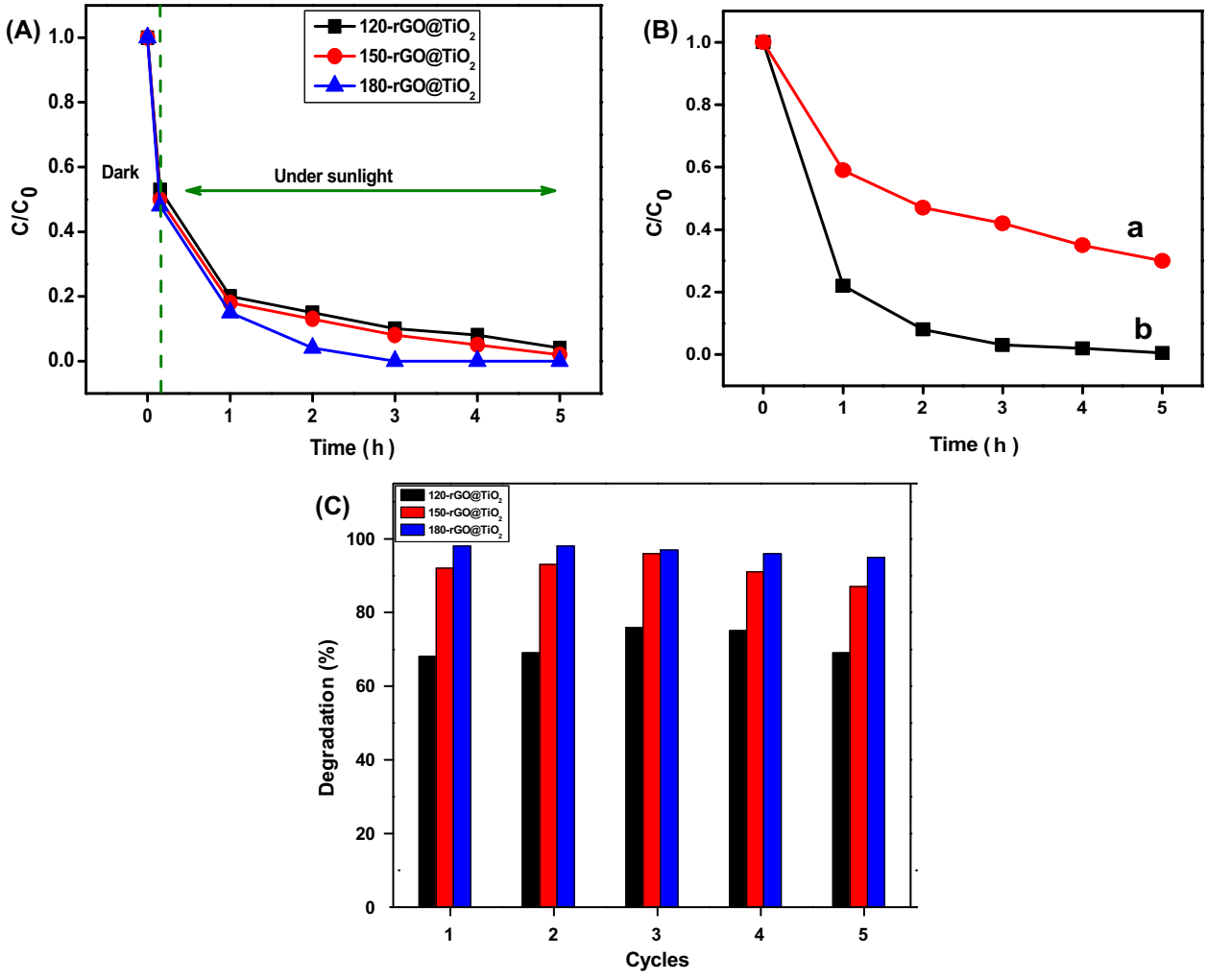


Fig. 6. (A) Photocatalytic degradation of MB in the presence of rGO–$TiO_2$ nanocomposites under natural sunlight irradiation. (B) Photocatalytic degradation of MB at 180-rGO–$TiO_2$ nanocomposite under (a) low and (b) high intensity of natural sunlight irradiation. (C) Sustainability of different rGO–$TiO_2$ nanocomposites up to five consecutive run under the identical experiments conditions.

conjugation between aromatic molecules and CNTs [38–40]. Among the three samples, the adsorption in the darkness exhibited an increasing trend in the order of 180-rGO–$TiO_2$, 150-rGO–$TiO_2$, and 120-rGO–$TiO_2$. Under natural solar light irradiation, ~80% of the dyes were decomposed by all three rGO–$TiO_2$ after 1 h. After 3 h irradiation, the 180-rGO–$TiO_2$ shows 100% degradation of MB. This may due to the better adsorptivity and rapid electron transfer in the nanocomposites (Fig. 6(A)). Moreover, the graphene acts as an electron acceptor and it hinders the electron-hole pair recombination efficiently. The photocatalytic experiments also carried out in the presence of the 180-rGO–$TiO_2$ nanocomposite under both low (15 $\mu W/cm^2$) and high (120 $\mu W/cm^2$) intensity of sunlight irradiation (Fig. 6(B)). The photocatalytic degradation of MB under low intensity was very poor (25.5%) even up to 5 h of irradiation. In contrast, the high intensity irradiation shows 98.8% degradation of MB. Hence, the effective photodegradation process not only due to adsorption of MB molecules on the catalyst surface and also depends on the intensity of the irradiation source.

Reusability of the catalyst is crucial for any heterogeneous catalyzed reaction, but some of the researchers have taken effort to test the reusability of powder photocatalysts. Owing to the difficulties in physical separation of the photocatalysts after pollutant degradation and also be due to the low sustainability of the catalysts. Present photocatalysts are easily separable from the solution and also well dispersible under stirring. It can be readily separate the photocatalyst from the cleaned solution by centrifugation and was no permanent adsorption of dye over the photocatalysts, and then removed only by photodegradation. Regeneration of the best photocatalyst, 180-rGO–$TiO_2$ carried out by each photodegardation experiments by centrifugation method and washing with DI water in order to remove the any organic contaminants due to the MB. The photocatalytic activity of the 180-rGO–$TiO_2$ nanocomposite remains the same even up to five consecutive run of the experiments under the identical conditions (Fig. 6(C)).

## 4. Conclusions

The rGO–$TiO_2$ nanocomposites were prepared through hydrothermal method at different reaction temperatures in the presence of TEA and used for the photocatalytic degradation of MB under natural sunlight. The prepared rGO–$TiO_2$ nanocomposites were characterized by various suitable techniques, including XRD, TEM, Raman, XPS, and PL. The reaction temperature during the synthesis of the rGO–$TiO_2$ nanocomposites plays a crucial role in controlling the structure and photocatalytic properties. Increasing the hydrothermal temperature to 180˚C allows the formation of more homogeneous composites with more quenching of PL. Among the various nanocomposites, the 180-rGO–$TiO_2$ nanocomposite shows better photodegradation efficiency toward the MB due to the narrow size distribution of $TiO_2$ nanoparticles, great adsorptivity of dyes, and low electron-hole pair recombination. Moreover, it shows good sustainability after subject to the five cycle of photocatlytic MB degradation. This work is anticipated to open a new possibility in the investigation of $TiO_2$–carbon composites and promote their practical application in addressing various environmental issues.

## Conflict of interests

The author(s) declare(s) that there is no conflict of interests regarding the publication of this paper.

## Acknowledgments

This work was financially supported by the High Impact Research Grant from the University of Malaya, the High Impact Research Grant (UM.S/P/HIR/MOHE/21) from the Ministry of Higher Education Malaysia, UMRG program grant (RP007C/13AFR) from the University of Malaya. BYS Chang would like to thank The Bright Sparks Unit of University of Malaya for the research incentives.

## References

[1] M.R. Hoffmann, S.T. Martin, W. Choi, D.W. Bahnemann, Environmental applications of semiconductor photocatalysis, Chem. Rev. 95 (1995) 69–96.
[2] A. Fujishima, T.N. Rao, D.A. Tryk, Titanium dioxide photocatalysis, J. Photochem. Photobiol. C 1 (2000) 1–21.
[3] A.L. Linsebigler, G. Lu, J.T. Yates, Photocatalysis on $TiO_2$ surfaces: Principles, mechanisms, and selected results, Chem. Rev. 95 (1995) 735–758.
[4] D. Ravelli, M. Fagnoni, D. Dondi, A. Albini, Significance of $TiO_2$ photocatalysis for green chemistry, J. Adv. Oxid. Technol. 14 (2011) 40–46.
[5] J. Zhang, Y. Wu, M. Xing, S.A.K. Leghari, S. Sajjad, Development of modified N doped $TiO_2$ photocatalyst with metals, nonmetals and metal oxides, Energy Environ. Sci. 3 (2010) 715–726.
[6] M.R. Hoffmann, S.T. Martin, W. Choi, D.W. Bahnemann, Environmental applications of semiconductor photocatalysis, Chem. Rev. 95 (1995) 69–96.
[7] R. Dhanalakshmi, A. Pandikumar, R. Ramaraj, Functionalized silicate supported $TiO_2$–ZnO nanocomposite film and its application in simultaneous photocatalytic degradation of toxic molecules, Mater. Sci. Forum 764 (2013) 255–265.

[8] A.L. Linsebigler, G. Lu, J.T. Yates, Photocatalysis on $TiO_2$ surfaces: Principles, mechanisms, and selected results, Chem. Rev. 95 (1995) 735–758.
[9] D. Ravelli, M. Fagnoni, D. Dondi, A. Albini, Significance of $TiO_2$ photocatalysis for green chemistry, J. Adv. Oxid. Technol. 14 (2011) 40–46.
[10] J. Zhang, Y. Wu, M. Xing, S.A.K. Leghari, S. Sajjad, Development of modified N doped $TiO_2$ photocatalyst with metals, nonmetals and metal oxides, Energy Environ. Sci. 3 (2010) 715–726.
[11] R. Leary, A. Westwood, Carbonaceous nanomaterials for the enhancement of $TiO_2$ photocatalysis, Carbon 49 (2011) 741–772.
[12] X. An, J.C. Yu, Graphene-based photocatalytic composites, RSC Adv. 1 (2011) 1426–1434.
[13] S.Z. Butler, S.M. Hollen, L. Cao, Y. Cui, J.A. Gupta, H.R. Gutiérrez, T.F. Heinz, S.S. Hong, J. Huang, A.F. Ismach, E. Johnston-Halperin, M. Kuno, V.V. Plashnitsa, R.D. Robinson, R.S. Ruoff, S. Salahuddin, J. Shan, L. Shi, M.G. Spencer, M. Terrones, W. Windl, J.E. Goldberger, Progress, challenges, and opportunities in two-dimensional materials beyond graphene, ACS Nano 7 (2013) 2898–2926.
[14] L. Wang, X. Lu, S. Lei, Y. Song, Graphene-based polyaniline nanocomposites: Preparation, properties and applications, J. Mater. Chem. A 2 (2014) 4491–4509.
[15] Q. Xiang, J. Yu, M. Jaroniec, Graphene-based semiconductor photocatalysts, Chem. Soc. Rev. 41 (2012) 782–796.
[16] S. Morales-Torres, L.M. Pastrana-Martínez, J.L. Figueiredo, J.L. Faria, A.M.T. Silva, Design of graphene-based $TiO_2$ photocatalysts—A review, Environ. Sci. Pollut. Res. 19 (2012) 3676–3687.
[17] H.N. Lim, N.M. Huang, S.S. Lim, I. Harrison, C.H. Chia, Fabrication and characterization of graphene hydrogel via hydrothermal approach as a scaffold for preliminary study of cell growth, Int. J. Nanomed. 6 (2011) 1817–1823.
[18] J. Wang, Y. Hernandez, M. Lotya, J.N. Coleman, W.J. Blau, Broadband nonlinear optical response of graphene dispersions, Adv. Mater. 21 (2009) 2430–2435.
[19] D. Eder, A.H. Windle, Carbon–inorganic hybrid materials: The carbon-nanotube/$TiO_2$ interface, Adv. Mater. 20 (2008) 1787–1793.
[20] H. Cao, Y. Zhu, X. Tan, H. Kang, X. Yang, C. Li, Fabrication of $TiO_2$/CdS composite fiber via an electrospinning method, New J. Chem. 34 (2010) 1116–1119.
[21] F. Tuinstra, J.L. Koenig, Raman spectrum of graphite, J. Chem. Phys. 53 (1970) 1126–1130.
[22] S. Stankovich, D.A. Dikin, R.D. Piner, K.A. Kohlhaas, A. Kleinhammes, Y. Jia, Y. Wu, S.T. Nguyen, R.S. Ruoff, Synthesis of graphene-based nanosheets via chemical reduction of exfoliated graphite oxide, Carbon 45 (2007) 1558–1565.
[23] O. Akhavan, M. Abdolahad, Y. Abdi, S. Mohajerzadeh, Synthesis of titania/carbon nanotube heterojunction arrays for photoinactivation of *E. coli* in visible light irradiation, Carbon 47 (2009) 3280–3287.
[24] L.C. Chen, Y.C. Ho, W.S. Guo, C.M. Huang, T.C. Pan, Enhanced visible light-induced photoelectrocatalytic degradation of phenol by carbon nanotube-doped $TiO_2$ electrodes, Electrochim. Acta 54 (2009) 3884–3891.
[25] O. Akhavan, E. Ghaderi, Photocatalytic reduction of graphene oxide nanosheets on $TiO_2$ thin film for photoinactivation of bacteria in solar light irradiation, J. Phys. Chem. C 113 (2009) 20214–20220.
[26] O. Akhavan, R. Azimirad, S. Safa, M.M. Larijani, Visible light photo-induced antibacterial activity of CNT-doped $TiO_2$ thin films with various CNT contents, J. Mater. Chem. A 20 (2010) 7386–7392.
[27] X. Cao, G. Tian, Y. Chen, J. Zhou, W. Zhou, C. Tian, H. Fu, Hierarchical composites of $TiO_2$ nanowire arrays on reduced graphene oxide nanosheets with enhanced photocatalytic hydrogen evolution performance, J. Mater. Chem. A 2 (2014) 4366–4374.
[28] L. Zhang, X. Li, Y. Huang, Y.F. Ma, X.J. Wan, Y.S. Chen, Controlled synthesis of few-layered graphene sheets on a large scale using chemical exfoliation. Carbon 48 (2010) 2367–2371.
[29] A.V. Murugan, T. Muraliganth, A. Manthiram, Rapid, facile microwave-solvothermal synthesis of graphene nanosheets and their polyaniline nanocomposites for energy strorage, Chem. Mater. 21 (2009) 5004–5006.
[30] Z.W. Xu, Y.D. Huang, C.Y. Min, L. Chen, Effect of $\gamma$-ray radiation on the polyacrylonitrile based carbon fibers, Radiat. Phys. Chem. 79 (2010) 839–843.
[31] G. Wang, Hydrothermal synthesis and photocatalytic activity of nanocrystalline $TiO_2$ powders in ethanol-water mixed solutions, J. Mol. Catal. A: Chem. 274 (2007) 185–191.
[32] Y.J. Xu, Y.B. Zhuang, X.Z. Fu, New insight for enhanced photocatalytic activity of $TiO_2$ by doping carbon nanotubes: A case study on degradation of benzene and methyl orange, J. Phys. Chem. C 114 (2010) 2669–2676.
[33] Y. Yao, G.H. Li, S. Ciston, R.M. Lueptow, K.A. Gray, Photoreactive $TiO_2$/carbon nanotube composites: Synthesis and reactivity, Environ. Sci. Technol. 42 (2008) 4952–4957.
[34] Y. Yu, J.C. Yu, C.Y. Chan, Y.K. Che, J.C. Zhao, L. Ding, W.K. Ge, P.K. Wong, Enhancement of adsorption and photocatalytic activity of $TiO_2$ by using carbon nanotubes for the treatment of azo dye, Appl. Catal. B 61 (2005) 1–11.
[35] K. Woan, G. Pyrgiotakis, W. Sigmund, Photocatalytic carbon-nanotube-$TiO_2$ composites, Adv. Mater. 21 (2009) 2233–2239.
[36] R. Czerw, B. Foley, D. Tekleab, A. Rubio, P.M. Ajayan, D.L. Carroll, Substrate-interface interactions between carbon nanotubes and the supporting substrate, Phys. Rev. B 66 (2002) 033408.
[37] Y. Xu, M.A.A. Schoonen, The absolute energy positions of conduction and valence bands of selected semiconducting minerals, Am. Mineral. 85 (2000) 543–556.
[38] H. Zhang, X.J. Lv, Y.M. Li, Y. Wang, J.H. Li, P25-graphene composite as a high performance photocatalyst, ACS Nano 4 (2010) 380–386.
[39] Z. Liu, J.T. Robinson, X.M. Sun, H.J. Dai, PEGylated nanographene oxide for delivery of water-insoluble cancer drugs, J. Am. Chem. Soc. 130 (2008) 10876–10877.
[40] P.S. Teo, A. Pandikumar, N.M. Huang, H.N. Lim, C.H. Chia, Magnetically separable reduced graphene oxide/iron oxide nanocomposite materials for environmental remediation, Catal. Sci. Technol. 4 (2014) 4396–4405.